Electronic Supplementary Material (ESI) for Dalton Transactions.
This journal is © The Royal Society of Chemistry 2022

$FeCoS_2$ polyhedral spherical nanoparticles decorated Nitrogen doped hollow carbon nanofibers as high-performance self-supporting anode for K-ion storage

Haoshan Xu [a], Shuhong Huang [a], Yang Yang [a], Jintao Chen [a], Lingxun Liang [b], Jun Zhang [b], Ling Li [a, *], Xiaohui Zhao [a, *], Wenming Zhang [a, *]

[a] *Province-Ministry Co-construction Collaborative Innovation Center of Hebei Photovoltaic Technology, College of Physics Science and Technology, Hebei University, Baoding, Hebei 071002, China.*

[b] *Drilling and Production Technology Research Institute of Liaohe Oilfield，PetroChina Liao he Oilfield Company, Panjin, Liaoning 124000, China.*

Corresponding author at:

E-mail: lilinghbu@163.com (L. Li), xhzhao@hbu.edu.cn (X. Zhao), wmzhang@hbu.edu.cn (W. Zhang).

Figures Captions:

Fig. S1. SEM images of (a) pure nanofibers, (b) an magnified SEM of pure nanofibers, (c) carbonized nanofibers, (d) an magnified SEM of carbonized nanofibers, (e) $FeCoS_2$@N-CNFs and (f) an magnified SEM of (e).

Fig. S2. SEM images of (a) pure coaxial nanofibers, (b) an magnified SEM of pure coaxial nanofibers, (c) carbonized hollow carbon nanofibers, (d) an magnified SEM of carbonized hollow carbon nanofibers.

Fig. S3. Energy dispersive spectrometer (EDS) of $FeCoS_2$@N-HCNFs.

Fig. S4. (a) Nitrogen adsorption-desorption isotherm curve and (b) pore diameter distribution image of the $FeCoS_2$@N-CNFs. (c) Nitrogen adsorption-desorption isotherm curve and (d) pore diameter distribution image of the HCNTs.

Fig. S5. Galvanostatic discharge/charge curves for the initial five cycles at 100 mA g^{-1} for (a) the $FeCoS_2$@N-CNFs and (b) the HCNTs electrodes.

Fig. S6. Nyquist plot of EIS profiles of FeCoS2@N-HCNFs, FeCoS2@N-CNFs and HCNFs anodes after 25 cycles.

Fig. S7. Relationship between real impedance (Z') and radial frequency ($\omega^{-1/2}$).

Fig. S8. Reaction mechanism diagram of $FeCoS_2$@N-HCNFs negative electrode.

Fig. S9. (a) CV curves of $FeCoS_2$@N-CNFs at various scan rate. (b) The connection between peak current and scan rate in KIBs is used to calculate the b value. (c) At a scan rate of 0.5 mV s^{-1} in KIBs, the CV curve of $FeCoS_2$@N-CNFs with the pseudocapacitive percentage represented by the covered areas. (d) Capacitive contribution percentage at various scan rate.

Fig. S10. TEM and HRTEM images of $FeCoS_2$@N-HCNFs electrode (a, d) discharge to 0.64 V, (b, e) discharge to 0.01 V, and (e, f) charge to 1.18V.

Fig. S11. SEM images of (a, b) fresh electrode, (c, d) $FeCoS_2$@N-HCNFs electrode after 5 cycles at 100 mA g^{-1} and (e, f) $FeCoS_2$@N-HCNFs electrode after 50 cycles at 100 mA g^{-1}.

Tables Captions:

Table S1. The comparison of electrochemical performance between $FeCoS_2$@N-HCNFs and other previously reported anode materials for KIBs.

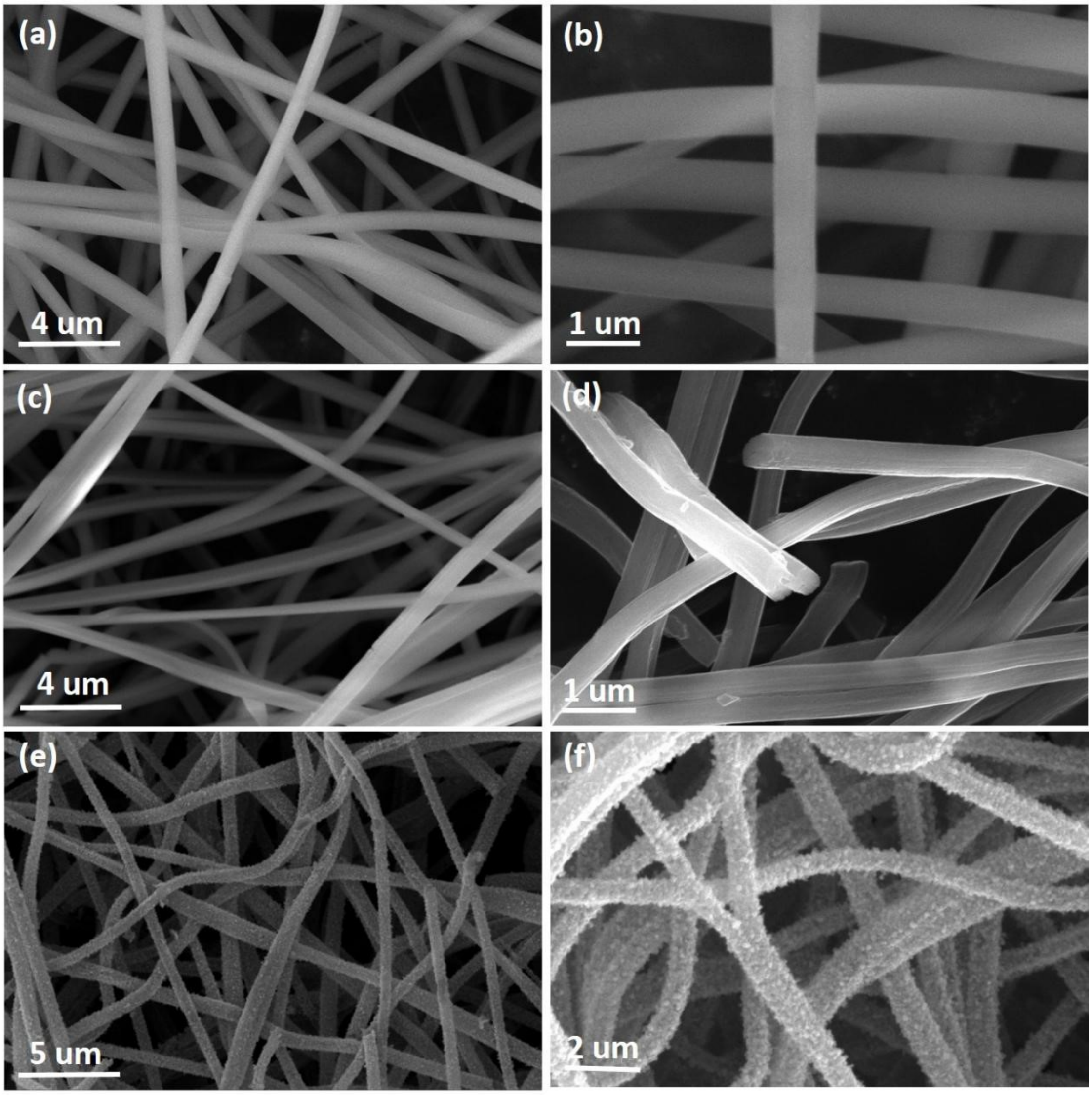

Fig. S1. SEM images of (a) pure nanofibers, (b) an magnified SEM of pure nanofibers, (c) carbonized nanofibers, (d) an magnified SEM of carbonized nanofibers, (e) $FeCoS_2$@N-CNFs and (f) an magnified SEM of (e).

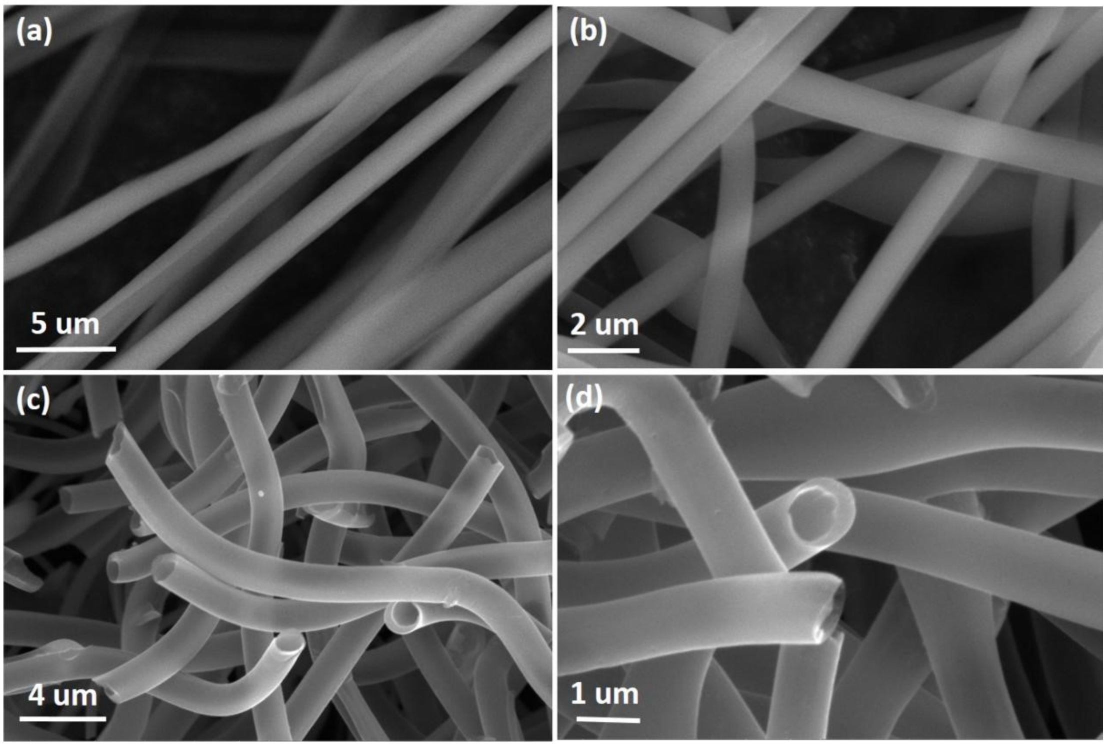

Fig. S2. SEM images of (a) pure coaxial nanofibers, (b) an magnified SEM of pure coaxial nanofibers, (c) carbonized hollow carbon nanofibers, (d) an magnified SEM of carbonized hollow carbon nanofibers.

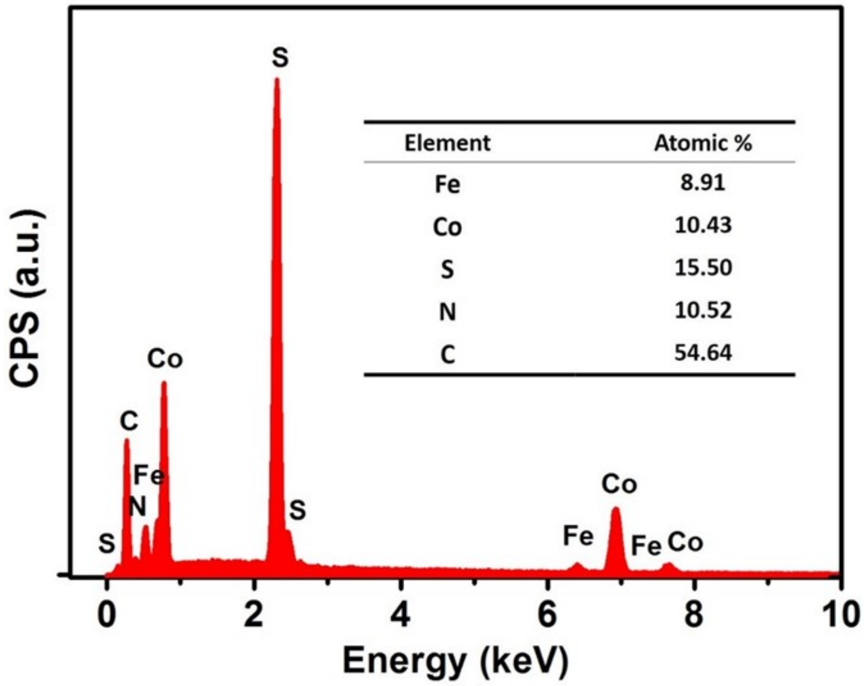

Fig. S3. Energy dispersive spectrometer (EDS) of $FeCoS_2$@N-HCNFs.

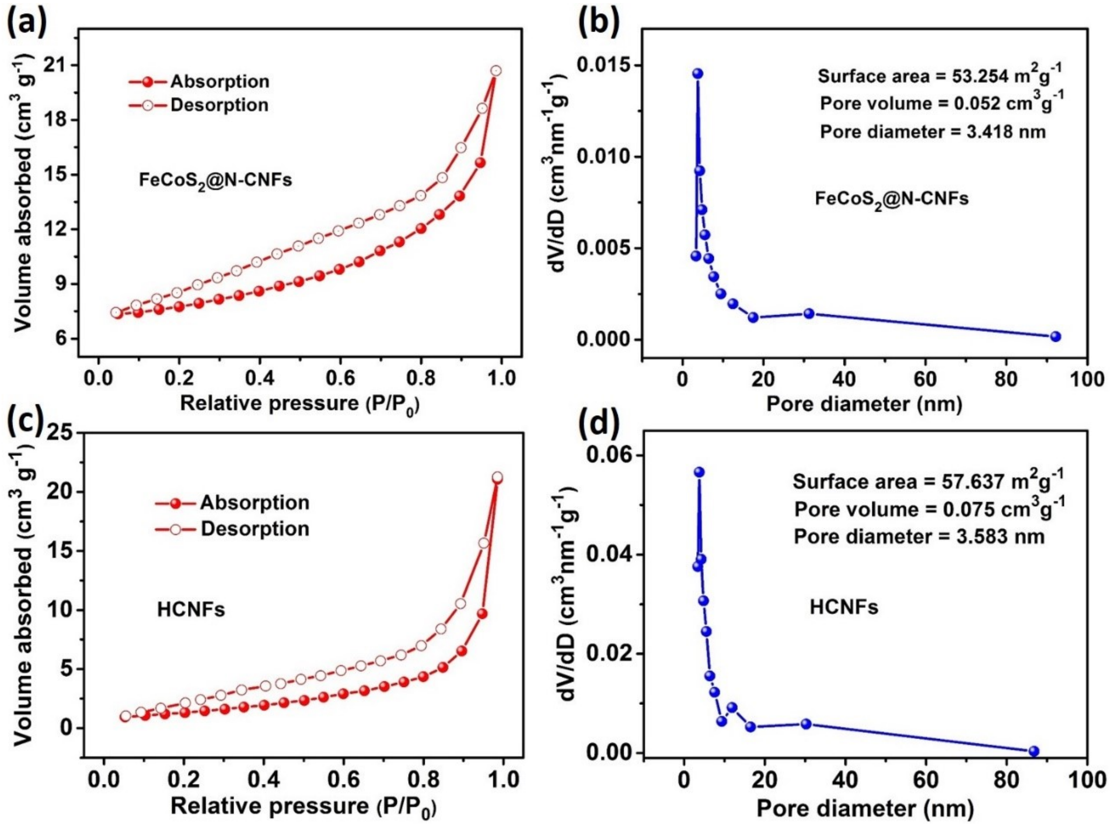

Fig. S4. (a) Nitrogen adsorption-desorption isotherm curve and (b) pore diameter distribution image of $FeCoS_2$@N-CNFs. (c) Nitrogen adsorption-desorption isotherm curve and (d) pore diameter distribution image of HCNFs

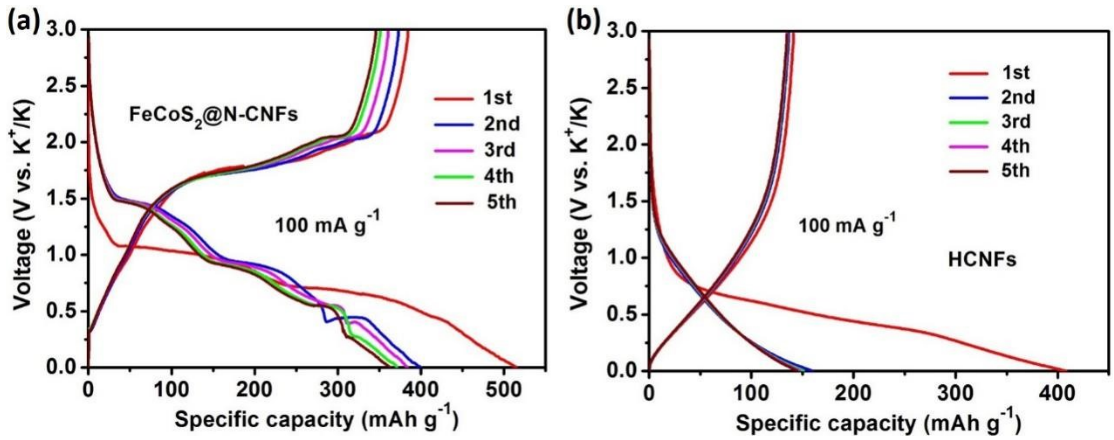

Fig. S5. Galvanostatic discharge/charge curves for the initial five cycles at 100 mA g^{-1} for (a) the $FeCoS_2$@N-CNFs and (b) the HCNFs electrodes.

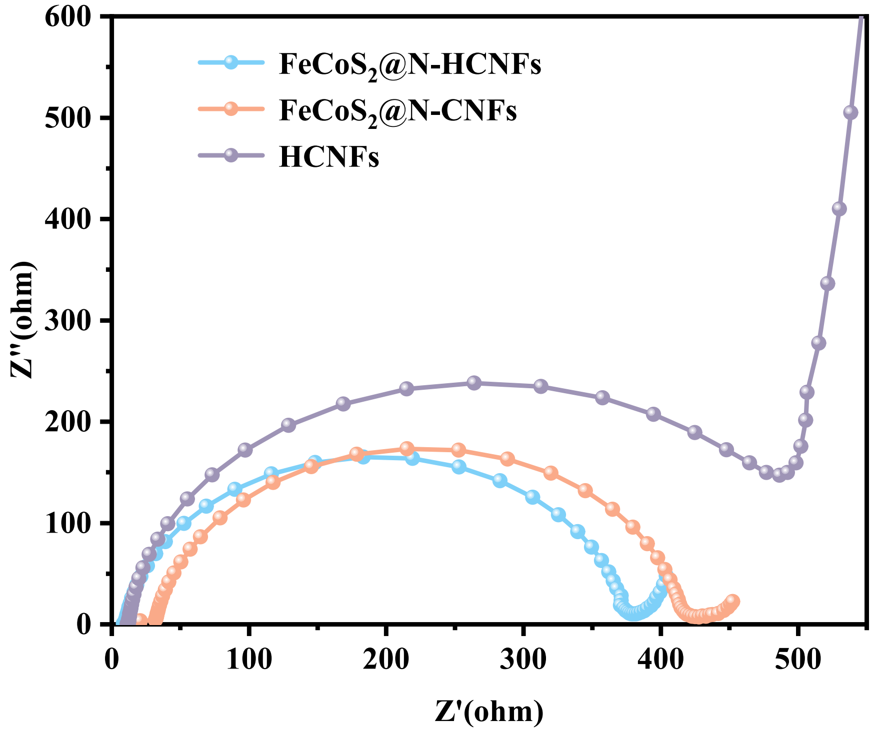

Fig. S6. Nyquist plot of EIS profiles of $FeCoS_2$@N-HCNFs, $FeCoS_2$@N-CNFs and HCNFs anodes after 25 cycles.

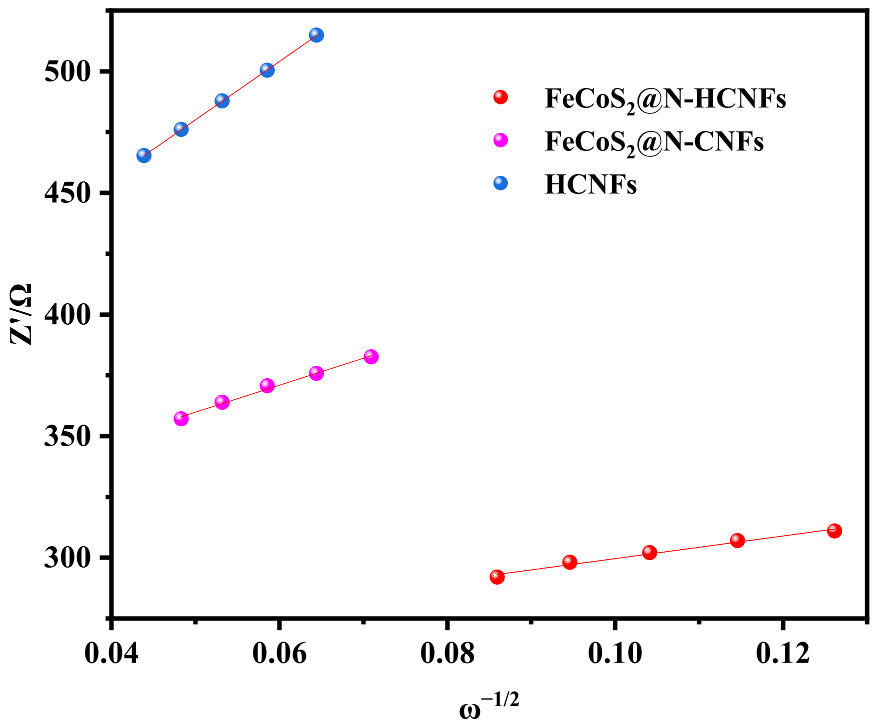

Fig. S7. Relationship between real impedance (Z’) and radial frequency ($\omega^{-1/2}$).

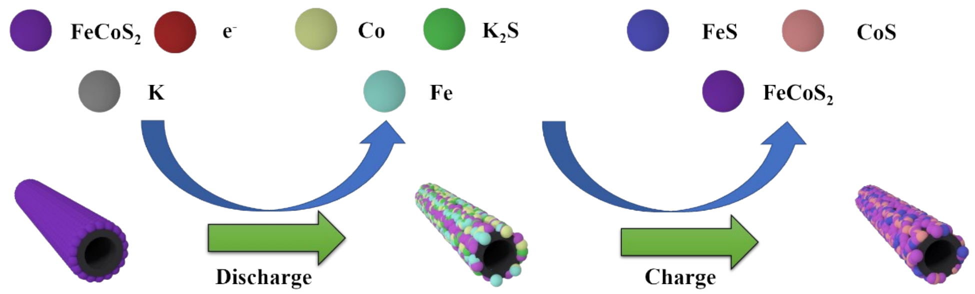

Fig. S8. Reaction mechanism diagram of $FeCoS_2$@N-HCNFs negative electrode.

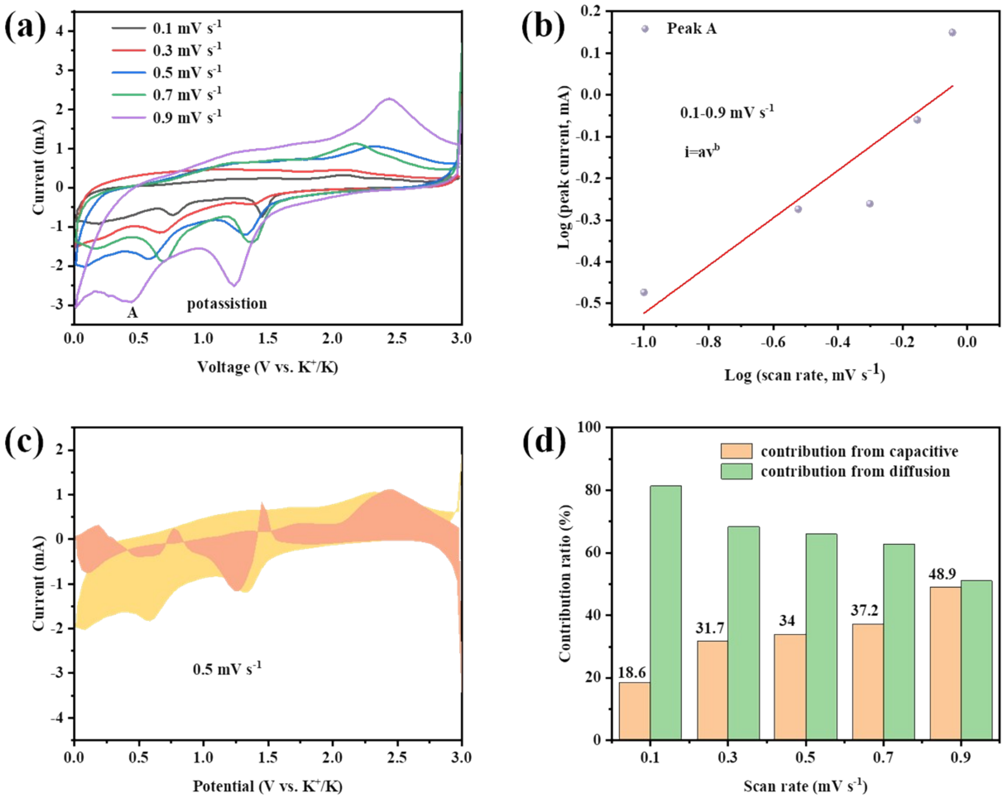

Fig. S9. (a) CV curves of $FeCoS_2$@N-CNFs at various scan rate. (b) The connection between peak current and scan rate in KIBs is used to calculate the b value. (c) At a scan rate of 0.5 mV s^{-1} in KIBs, the CV curve of $FeCoS_2$@N-CNFs with the pseudocapacitive percentage represented by the covered areas. (d) Capacitive contribution percentage at various scan rate.

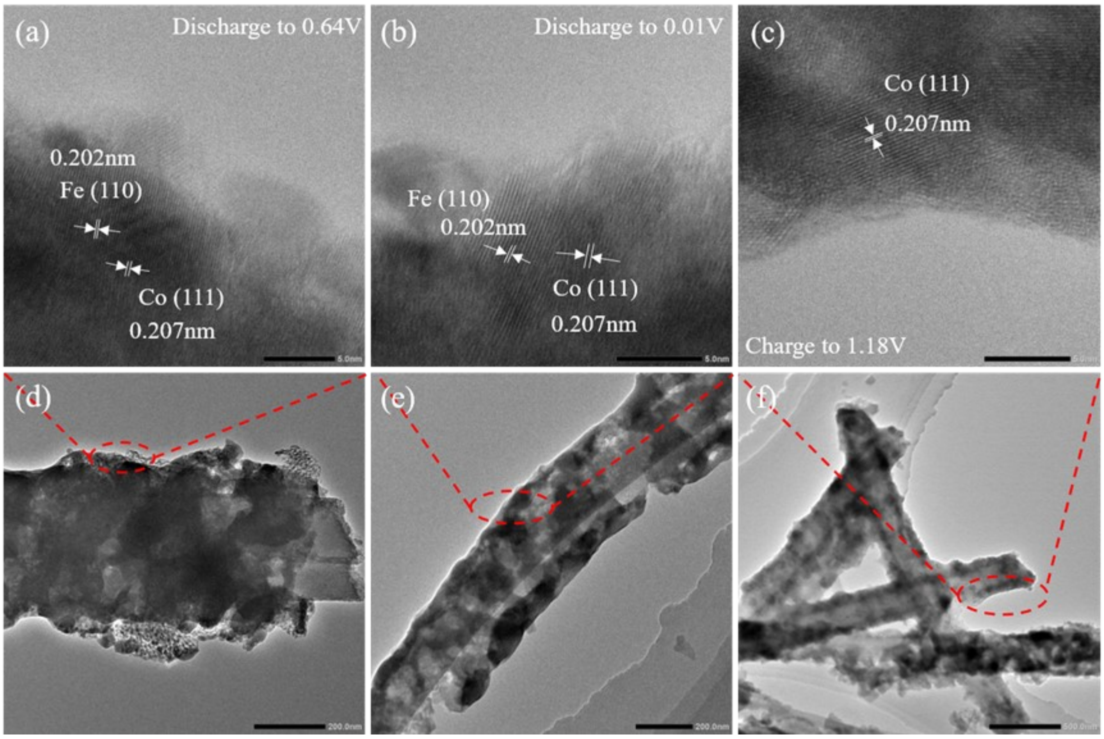

Fig. S10. TEM and HRTEM images of $FeCoS_2$@N-HCNFs electrode (a, d) discharge to 0.64 V, (b, e) discharge to 0.01 V, and (e, f) charge to 1.18V.

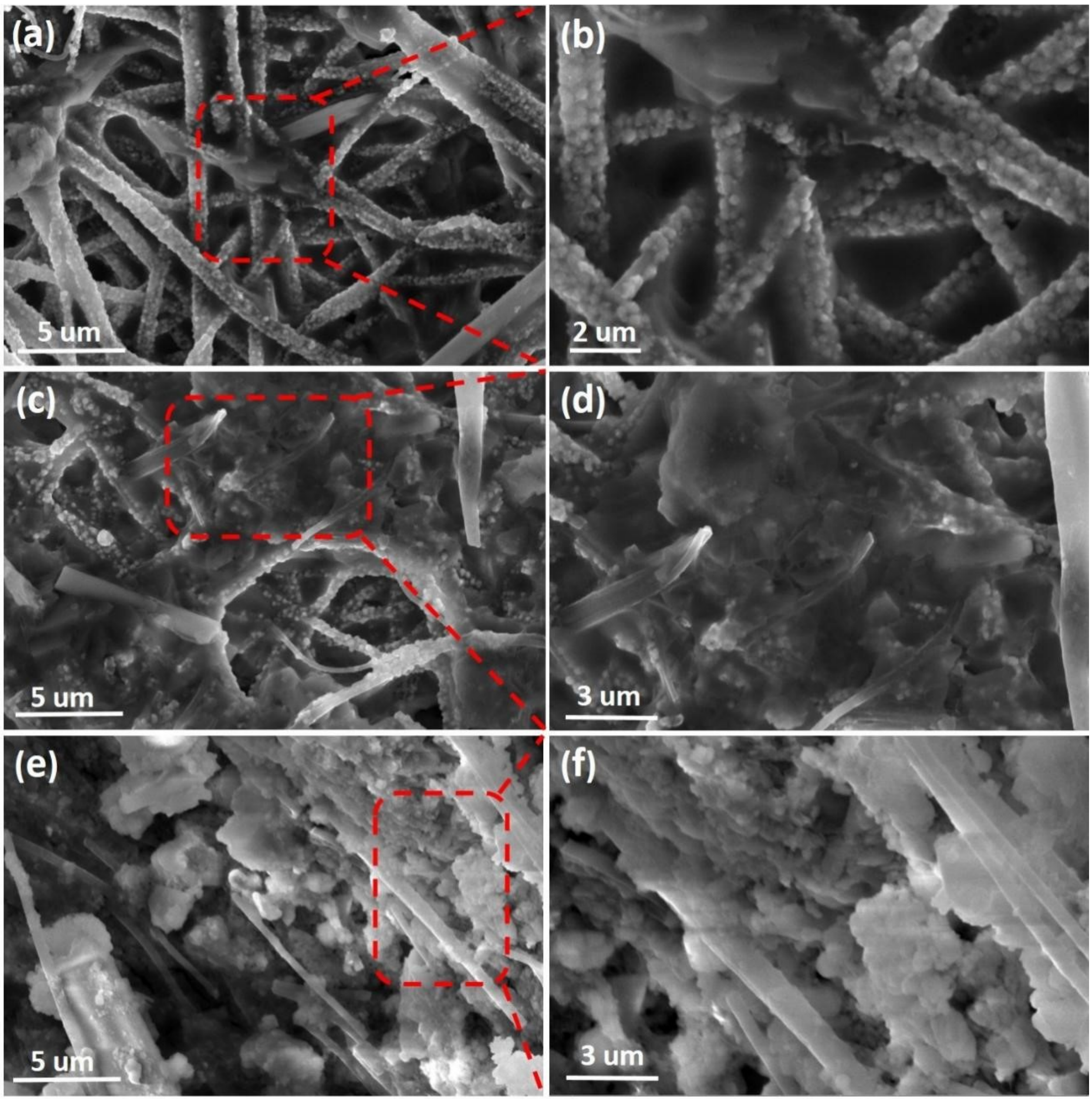

Fig. S11. SEM images of (a, b) fresh electrode, (c, d) $FeCoS_2$@N-HCNFs electrode after 5 cycles at 100 mA g^{-1} and (e, f) $FeCoS_2$@N-HCNFs electrode after 50 cycles at 100 mA g^{-1}.

Table S1. Comparison of the electrochemical potassium-storage properties of different carbon-based self-supporting anode materials in this work and previously reported nanomaterials.

Materials (Mass loading)	Current density (mA g^{-1})	Reversible capacity (mAh g^{-1})	Rate capacity (mAh g^{-1})	Ref/Year
NHC (0.6-1.4 mg/cm^2)	100	293.5 mA h g^{-1} (50 cycles)	204 mA h g^{-1} (2000 mA g^{-1})	[1]/2019
NCNTs (0.7 mg cm^{-2})	50	254.7 mA h g^{-1} (300 cycles)	180 mA h g^{-1} (500 mA g^{-1}) 102 mA h g^{-1} (2000 mA g^{-1})	[2]/2018
HCNTs (3.08 mg cm^{-2})	100	232 mA h g^{-1} (500 cycles)	162 mA h g^{-1} (1600 mA g^{-1})	[3]/2018
Porous CNF (1.5 mg/cm^2)	20	270 mA h g^{-1} (80 cycles)	190mA h g^{-1} (2000 mA g^{-1}) 140 mA h g^{-1} (5000 mA g^{-1}) 100 mA h g^{-1} (7700mA g^{-1})	[4]/2017
OMC	200	197.8 mA h g^{-1} (200 cycles)	286.4 mA h g^{-1} (50 mA g^{-1}) 255.1 mA h g^{-1} (100 mA g^{-1}) 186.3 mA h g^{-1} (500 mA g^{-1}) 144.2mA h g^{-1} (1000 mA g^{-1})	[5]/2018
N-FLG	100	210 mA h g^{-1} (100cycles)	350 mA h g^{-1} (50 mA g^{-1})	[6]/2016
HINCA (1.1~2 mg cm^{-2})	140	250 mA h g^{-1} (150 cycles)	340 mA h g^{-1} (28 mA g^{-1}) 300 mA h g^{-1} (56 mA g^{-1})	[7]/2018
Graphite	140	100 mA h g^{-1} (50 cycles)	80 mA h g^{-1} (270 mA g^{-1})	[8]/2015
CNTs/GCF	100	226 mA h g^{-1} (800 cycles)	254 mA h g^{-1} (50 mA g^{-1}) 233 mA h g^{-1} (100 mA g^{-1}) 204 mA h g^{-1} (200 mA g^{-1}) 113 mA h g^{-1} (500 mA g^{-1}) 74 mA h g^{-1} (1000 mA g^{-1})	[9]/2019
NCSCNT (1 mg/cm^2)	50	236 mA h g^{-1} (100 cycles)	150mA h g^{-1} (200 mA g^{-1}) 98 mA h g^{-1} (600 mA g^{-1}) 75 mA h g^{-1} (1000mA g^{-1})	[10]/2018
rGO/CNT-30%	50	223 mA h g^{-1} (200 cycles)	246 mA h g^{-1} (20 mA g^{-1}) 201 mA h g^{-1} (30 mA g^{-1}) 179 mA h g^{-1} (50 mA g^{-1}) 110 mA h g^{-1} (100 mA g^{-1})	[11]/2019
$FeCoS_2$@N-HCNFs (0.8-1.5 mg/cm^2)	100	238 mA h g^{-1} (200 cycles)	384.3 mA h g^{-1} (100 mA g^{-1}) 327.8 mA h g^{-1} (200 mA g^{-1}) 273.6 mA h g^{-1} (400 mA g^{-1}) 228.7 mA h g^{-1} (800 mA g^{-1}) 180.9 mA h g^{-1} (1600 mA g^{-1})	This work

References

[1] W.X. Yang, J.H. Zhou, S. Wang, W.Y. Zhang, Z.C. Wang, F. Lv, K. Wang, Q. Sun, S.J. Guo, Freestanding film made by necklace-like N-doped hollow carbon with hierarchical pores for high-performance potassium-ion storage, Energy Environ. Sci. 12 (2019) 1605-1612.

[2] P.X. Xiong, X.X. Zhao, Y.H. Xu, Nitrogen-doped carbon nanotubes derived from metal-organic frameworks for potassium-ion battery anodes, ChemSusChem. 11(1) (2018) 202–208.

[3] Y.S. Wang, Z.P. Wang, Z.P. Wang, Y.J. Chen, H. Zhang, M. Yousaf, H.S. Wu, M.C. Zou, A.Y. Cao, R.P.S. Han, Hyperporous sponge interconnected by hierarchical carbon nanotubes as a high-performance potassium-ion battery anode, Adv. Mater. 30(32) (2018) 1802074.

[4] X.X. Zhao, P.X. Xiong, J.F. Meng, Y.Q. Liang, J.W. Wang, Y.H. Xu, High Rate and Long Cycle Life Porous Carbon Nanofiber Paper Anodes for Potassium-Ion Batteries, J. Mater. Chem. A 36(5) (2017) 19237-19244.

[5] W. Wang, J.H. Zhou, Z.P. Wang, L.Y. Zhao, P.H. Li, Y. Yang, C. Yang, H.X. Huang, S.J. Guo, Short-Range Order in Mesoporous Carbon Boosts Potassium-Ion Battery Performance, Adv. Energy Mater. 8(5) (2018), 1701648.

[6] Keith Share, Adam P. Cohn, Rachel Carter, Bridget Rogers, Cary L. Pint, Role of Nitrogen-Doped Graphene for Improved High-Capacity Potassium Ion Battery Anodes, ACS Nano 10(25) (2016), 9738−9744.

[7] D.S. Bin, X.J. Lin, Y.G. Sun, Y.S. Xu, K. Zhang, A.M. Cao, L.J. Wan, Engineering Hollow Carbon Architecture for High-Performance K-Ion Battery Anode,

J. Am. Chem. Soc. 140(2018), 7127−7134.

[8] Z.L. Jian, W. Luo, X.L. Ji, Carbon electrodes for K-Ion batteries, J. Am. Chem. Soc. 137(36) (2015) 11566-11569.

[9] S.F. Zeng, X.F. Zhou, B. Wang, Y.Z. Feng, R. Xu, H.B. Zhang, S.M. Peng, Y. Yu, Freestanding CNT-modified graphitic carbon foam as a flexible anode for potassium ion batteries, J. Mater. Chem. A 26(7) (2019) 15774-15781.

[10] X.X. Zhao, Y.F. Tang, C.L. Ni, J.W. Wang, A. Star, Y.H. Xu, Free-standing nitrogen-doped cup-stacked carbon nanotube mats for potassium-ion battery anodes, ACS Appl. Energy Mater. 1(4) (2018) 1703−1707.

[11] S.T. Peng, L.C. Wang, Z.Q. Zhu, K. Han, Electrochemical performance of reduced graphene oxide/carbon nanotube hybrid papers as binder-free anodes for potassium-ion batteries, J. Phys. Chem. Solids. 138 (2020) 109296.